CrossMark

ORIGINAL PAPER

Tribological Behavior of a Cold-Sprayed Cu–MoS$_2$ Composite Coating During Dry Sliding Wear

Yinyin Zhang[1] · J. Michael Shockley[1] · Phuong Vo[2] · Richard R. Chromik[1]

Abstract Two cold spray coatings, one pure Cu and the other a Cu–MoS$_2$ composite coating, were studied for their tribology performance in dry air. It was demonstrated that a small amount of MoS$_2$ (1.8 ± 0.99 wt%) could significantly decrease coefficient of friction (CoF) from around 0.7 (Cu coating) to 0.14–0.15. MoS$_2$ patches on the wear track exhibited a lower local CoF, and the main velocity accommodation mechanism was shearing MoS$_2$-containing debris. Even though the coating wear rates were high in the early sliding (8.61–12.8 nm/cycle in penetration depth during the first 100 cycles), slow wear (0.12–0.22 nm/cycle) over the subsequent sliding was observed. It was also found that the presence of MoS$_2$ helped to achieve high endurance of the first steady-state CoF. The dynamics of the process, material transfer, and phase transformation were examined using scanning electron microscopy, energy-dispersive X-ray spectroscopy, and Raman spectroscopy. The MoS$_2$ patches developed on the wear track and the counterface served as reservoirs to replenish MoS$_2$ in the contact and became depleted with sliding. Cross-sectional microstructure revealed by electron channeling contrast imaging technique showed a layer of sliding-induced microstructure, 3–5 μm thick for the Cu–MoS$_2$ coating, and 10–30 μm thick for the Cu coating.

Keywords Cold spray · Metal matrix composite · Friction · Wear rate · MoS$_2$ · Subsurface microstructure

✉ Richard R. Chromik
richard.chromik@mcgill.ca

[1] Department of Mining and Materials Engineering, McGill University, Montreal, QC, Canada

[2] National Research Council Canada, 75, boul. de Mortagne, Boucherville, QC, Canada

1 Introduction

MoS$_2$ is a well-known solid lubricant and produces some of the lowest friction coefficients ever measured in vacuum and dry gas environments, where it also shows a long sliding life and low overall wear rates ($\ll 1$ nm/cycle) [1–3]. Therefore, composite materials consisting of dispersed MoS$_2$ in a metal matrix have received interest for their improved tribological performance [4]. Silver, iron, molybdenum, copper, and other metals and alloys have been used as metallic matrices and have been processed by sintering and hot-pressing with MoS$_2$, producing self-lubricating dry bearing materials where the friction coefficients vary in a range of 0.04–0.26 depending on MoS$_2$ concentration [4–6]. However, when MoS$_2$ exceeds a certain concentration, wear resistance decreases as well because of mechanical property losses. Dhanasekaran et al. [5] found optimized friction and wear resistance with no more than 3 % MoS$_2$ content. For coating applications, thermal spray is one of the most frequent technologies. WC–Co/MoS$_2$–Ni coatings showed improved friction compared to their metal matrix. Yet mechanical properties such as hardness and fracture toughness also decreased with MoS$_2$ content. The wear rate starts to climb once the MoS$_2$ exceeds 5 wt% [7, 8]. Similarly, improved friction was observed in thermal-sprayed WC–Co/Cu–MoS$_2$ coatings with MoS$_2$ concentration up to 12 wt%, but the 8 wt% MoS$_2$ coating showed the optimized wear rate [9].

In addition, the above manufacturing processes, for both bulk and coating materials, inevitably cause high-temperature-induced decomposition of MoS$_2$ and/or other phase transformations that could be detrimental for tribological performance [4, 6, 10]. Brittle compounds of Cu$_2$S and CuMo$_2$S$_3$ were commonly observed in sintered Cu–MoS$_2$ composites, causing MoS$_2$ to be ineffective as a solid

lubricant and thus resulting in high friction and wear [6, 10].

Cold spray is a relatively new coating deposition process where particles are fed to a de Laval nozzle, undergo acceleration to supersonic velocities (500–1200 m/s) and impact onto a substrate. In this process, the gas is preheated to temperatures below the melting temperature of sprayed materials [11–13]. Since high temperature is not involved, it is ideally applied for heat-sensitive materials such as solid lubricants and oxygen-sensitive materials like copper [11, 14, 15]. However, up to now only a few studies have been devoted to exploring the tribological behavior of metal-solid lubricant composites fabricated by cold spray [16, 17].

In the present study, cold spray was applied to develop a Cu–MoS$_2$ composite coating using admixed feedstock. Its tribological behavior was studied under dry sliding. Post-test observations including morphology and composition analysis on the wear tracks and counterfaces were conducted in order to better understand its friction mechanisms. The endurance of the first steady-state friction was also examined, with emphasis placed on the role of MoS$_2$.

2 Experimental

2.1 Cold Spray and Coating Characterization

A commercially available cold spray system (PCS800, Plasma Giken, Japan) was used to fabricate one Cu coating and one Cu–MoS$_2$ composite coating using the same deposition conditions. A spherical Cu powder (Tekna Advanced Materials Inc., $d_{50} = 26$ μm) and a flake-like MoS$_2$ powder (Climax, $d_{50} = 30$ μm) were used as feedstock (Fig. 1). For the composite coating, a mixture of 95 wt% Cu and 5 wt% MoS$_2$ was mechanically mixed for 1 h. Nitrogen was used as the process gas, and the gas pressure and preheat temperature were maintained at 5 MPa and 800 °C, respectively. Grit-blasted AA6061 aluminum alloy plates were used as substrates and were preheated up to around 170 °C immediately before coating deposition by traversing the spray gun over the substrate with the heated gas jet only, i.e., without feeding any powder. Preliminary studies indicated that a preheated substrate reduced porosity and enhanced deposition efficiency for the composite coating. The gun traverse speed was set at 60 mm/s, and the standoff distance at 40 mm.

Cross sections of the coatings were prepared by grinding, polishing, and a final step of vibratory polishing using colloidal silica (0.05 μm) for 3 h. MoS$_2$ concentration within the composite coating was measured by image analysis through pixel count using ten scanning electron microscope (SEM) images with a magnification of 1000×.

2.2 Sliding Wear Tests

Sliding wear tests on both pure Cu and Cu + MoS$_2$ composite coatings were conducted in dry air (0 % relative humidity) at room temperature (21–24 °C) using a custom-built reciprocating tribometer [18]. Friction forces were measured using a piezoelectric sensor at a sampling rate of 800 Hz. Polycrystalline α-Al$_2$O$_3$ balls of 6.35 mm diameter were used as counterfaces and were loaded with a normal load of 5 N onto the coatings. All sliding tests were performed at a speed of 2 mm/s and a track length of 4 mm. Most of the tests were conducted up to 1000 cycles. In order to examine the intermediate state and endurance of the first steady state, short and long tests to 100 and 3000 cycles, respectively, were also conducted.

2.3 Analysis of Wear Tracks and Counterfaces

After sliding wear tests, a Wyko NT8000 non-contact optical profiler was used to obtain surface topography, from which cross-sectional profiles of wear tracks were extracted. The depth of the wear tracks were subsequently obtained and used to calculate wear rate in terms of the rate of penetration depth in nm/cycle. An excess of 30 cross sections were extracted from each wear track in order to minimize the uncertainty in wear rate calculation.

The wear track morphologies were studied by a cold field emission SEM (Hitachi, SU-8230, Japan), and elemental composition was revealed by energy-dispersive X-ray spectroscopy (EDX). An inVia Raman microscope (Renishaw, UK) equipped with an Ar$^+$ ion ($\lambda = 514.5$ nm) laser source was used to identify phase composition on the wear tracks and counterfaces. Subsurface regions of the wear tracks were studied by cutting them transversely to the sliding direction using a lubricated slow-speed precision diamond sectioning blade, followed by cold-mounting, mechanical grinding and polishing, and finally Ar$^+$ ion milling. Using a photodiode semiconductor BSE detector, electron channeling contrast imaging (ECCI) observations were carried out to reveal grains and other defects.

3 Results

3.1 Cold-Sprayed Coatings

A cross section of the as-sprayed Cu–MoS$_2$ composite coating shows dark contrast around the particles (Fig. 1a), which was identified as MoS$_2$ by EDX mapping (Fig. 1b). As shown in Fig. 1a, where region A contains more MoS$_2$ than region B, local MoS$_2$ content varies throughout the coating. The average MoS$_2$ concentration was measured as 1.8 ± 0.99 wt%.
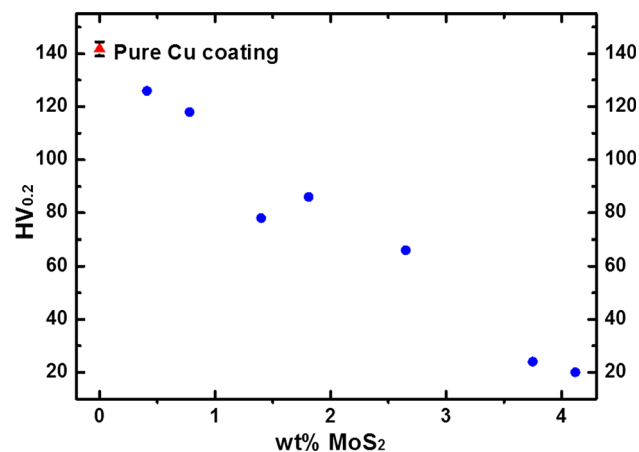
Fig. 1 a Cross-sectional morphology; **b** EDX maps of the distribution of Cu, Mo, and S of the rectangle area; **c**, **d** indents of microhardness tests on the corresponding regions denoted as *A* and *B* in (**a**)
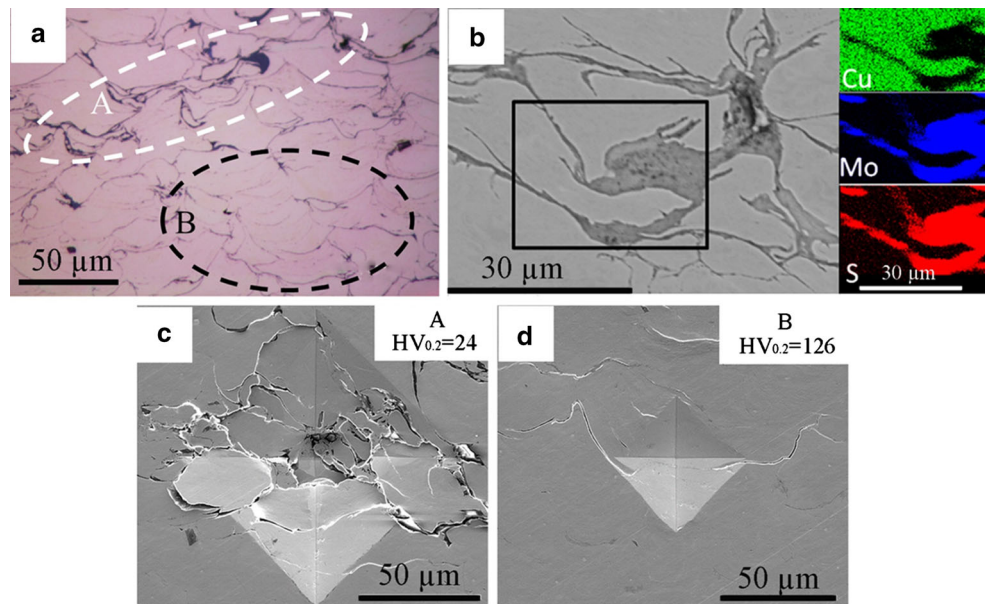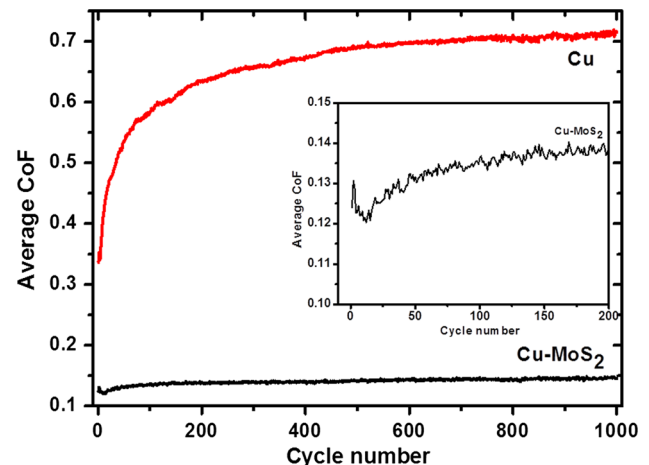
As revealed by microhardness tests on regions of varying MoS_2 concentration (Fig. 1c, d), higher local MoS_2 content led to much lower local hardness because of particle de-bonding. This implies bonding strength between particles was weak due to the presence of MoS_2. Over the range of local MoS_2 concentrations found within the composite coating, in addition to the hardness measurement of the pure Cu coating, the hardness decreased linearly with MoS_2 concentration (Fig. 2).

3.2 Average Friction

The average friction coefficient (CoF) versus cycle numbers is shown in Fig. 3, where Cu–MoS_2 and Cu
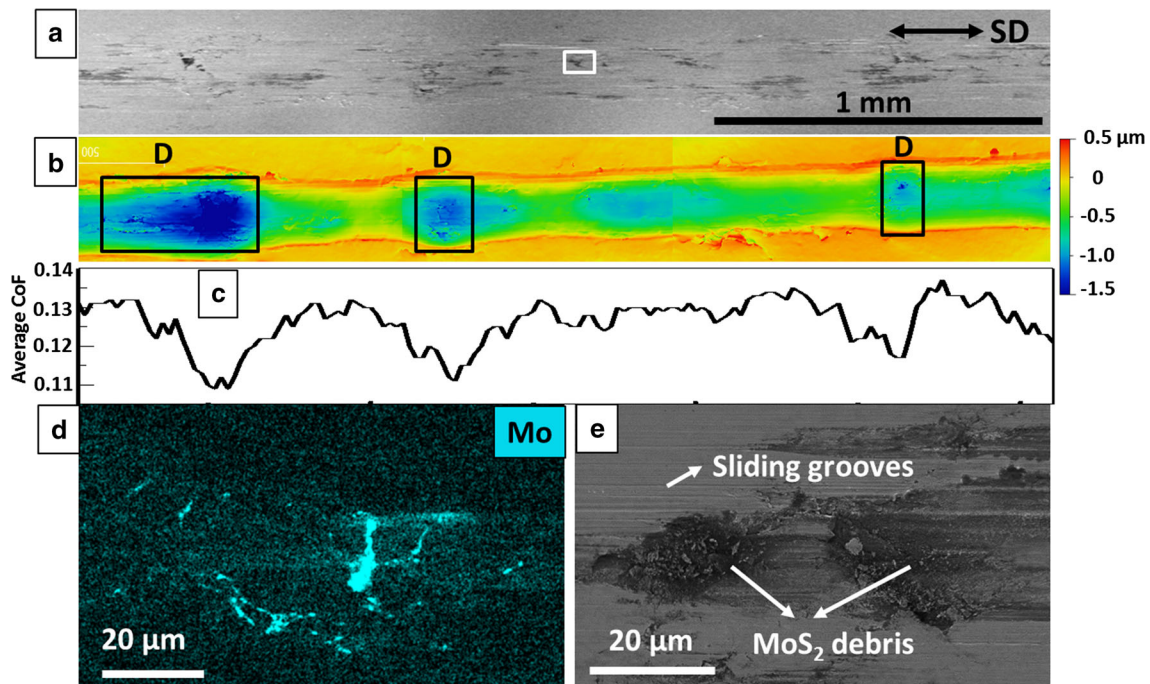

Fig. 3 Average coefficient of friction versus cycle number of cold-sprayed Cu–MoS_2 and Cu coatings. *Inset* is a closer view of the beginning of CoF versus cycle number for Cu–MoS_2 coating

coatings exhibited different friction behavior. Cu–MCu–MoS_2 coating showed a much lower CoF overall. After a short run-in stage of around 50 cycles (see the inset), where CoF decreased slightly, then increased gradually, and eventually stayed constant between 0.14 and 0.15, the Cu coating showed a continuous increase in CoF over the first 400 cycles until reaching the steady-state value of roughly 0.7.

3.3 Morphology and Local Friction Measurements

Figure 4a shows a top-down observation on the Cu–MoS_2 wear track after a 100 cycle test. It reveals dark contrast throughout the whole wear track. In Fig. 4d, an EDX map

Fig. 2 Microhardness varies with MoS_2 concentration: microhardness linearly decreased with MoS_2 concentration and pure Cu coating shows the highest hardness

Fig. 4 Top-down view of the Cu–MoS$_2$ wear track after a 100 cycle test. **a** Overall morphology; **b** wear track topography, where the *rectangles* indicate deep zones (denoted as *D*); **c** spatial friction along the wear track at the 100th cycle; **d** an EDX map of the *white rectangle* in (**a**); **e** a closer view of the wear track morphology. Refer to the scale bar in **a** for **a**, **b**, and **c**. SD indicates sliding direction

of the dark contrast region shows that it corresponds to Mo-rich zones that are indicative of MoS$_2$. According to the Mo count distribution, the brightest areas have the highest MoS$_2$ content, which might be particle boundaries originally (Fig. 1a, b). Around those bright areas, lower counts of Mo were detected. Figure 4e is a closer view of the morphology of such a zone, where MoS$_2$ was observed as fine debris. Sliding grooves were found in the region that was not covered by the debris. Figure 4c plots spatial friction at the 100th cycle with values fluctuating between 0.11 and 0.135. It also shows some zones exhibiting lower friction. Topography of the wear track is shown in Fig. 4b, which exhibited wavy boundaries and local variations in the track depth. The deeper zones showed lower local friction, as seen in Fig. 4b, c, and that was due to the presence of MoS$_2$ patches (Fig. 4a).

After 1000 cycles, as shown in Fig. 5a, the wear track became relatively uniform and the MoS$_2$ patches seen in the 100-cycle wear track were not found. Instead, a relatively homogeneous distribution of Mo was observed by EDX map (Fig. 5d), indicating MoS$_2$ tended to be evenly distributed during sliding. In Fig. 5e, the powdery morphology suggests MoS$_2$ manifested as fine debris and could be further mixed over sliding. Nevertheless, the wear track depth still locally varied, and it was found that the deeper zones tended to exhibit a lower coefficient of friction (Fig. 5b, c).

For the pure Cu coating, the wear track after a 100 cycle test exhibited a relatively uniform feature including morphology (Fig. 6a, d) and topography (Fig. 6b). A closer view of the wear track (Fig. 6d) shows continuous sliding grooves parallel to the sliding direction. In terms of penetration depth, compared to the Cu–MoS$_2$ wear track, the Cu wear track was more uniform and shallower (Fig. 6b). The spatial friction along the wear track at 100 cycles, shown in Fig. 6c, did not show the pattern obtained in the Cu–MoS$_2$ coating. At 1000 cycles, uniform features such as wear track morphology and topography were observed (Fig. 7a–c, respectively). Continuous sliding grooves parallel to the sliding direction were observed exclusively in the wear track (Fig. 7b), yet extruded wear debris was found along both track boundaries (Fig. 7a). It is worth noting that a uniformly distributed fluctuation in friction at 1000 cycles was observed, which was probably due to surface roughness-induced vibration.

3.4 Wear

Inhomogeneous wear tracks were generated in the Cu–MoS$_2$ composite coating (Figs. 4b, 5b), where deeper zones corresponded to higher MoS$_2$ concentrations with poor mechanical properties (Fig. 2). To explore variations in the coating performance due to local MoS$_2$ concentration, the wear track was divided into two classes based on
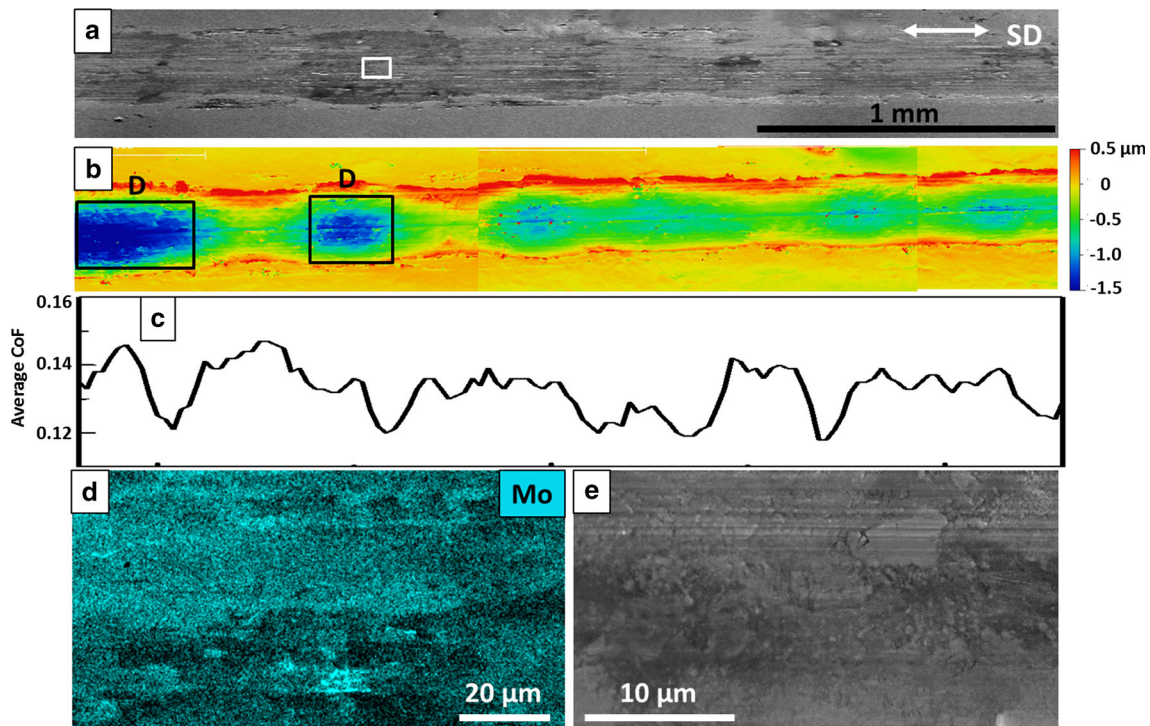
Fig. 5 Top-down view of the Cu–MoS$_2$ wear track after a 1000 cycle test. **a** Overall morphology; **b** wear track topography, where the *rectangles* indicate deep zones (denoted as *D*); **c** spatial friction along the wear track at the 1000th cycle; **d** an EDX map of the *white rectangle* in (**a**); **e** a closer view of the wear track morphology. Refer to the scale bar in **a** for **a**, **b**, and **c**. SD indicates sliding direction

the local depth, and wear rates for each class were calculated separately. As shown in Fig. 4b, the rectangles labelled "D" identified deep zones; other areas were shallow zones (noted as "S" afterward). D zones, with sliding up to 1000 cycles, shown as rectangles in Fig. 5b, were defined as the areas where wear track depth was greater than those D zones at 100 cycles. The evolution of the wear track depth of "D" and "S" zones as well as that of the pure Cu coating is shown in Fig. 8, where wear track depth increased with MoS$_2$ content and cycle number. At 100 cycles, D zones, which have more MoS$_2$, generated the deepest wear track of around 1.28 μm in average, while 0.86 μm deep for the S zones, where less MoS$_2$ was found. The pure Cu coating shows the shallowest wear track of roughly 0.20 μm in depth. Similarly, at 1000 cycles, D zones formed the deepest wear track, followed by S zones and finally the pure Cu coating. Subsequently, wear rates were calculated in terms of rate of penetration depth, as shown in Table 1. After the first 100 cycles, the Cu–MoS$_2$ coating was worn faster. A higher wear rate (12.8 ± 3.41 nm/c) occurred in D zones followed by S zones (8.61 ± 3.15 nm/c), while the pure Cu coating showed mild wear of 2.04 ± 0.31 nm/c. However, during the subsequent 900 cycles, D and S zones showed very low and similar wear rates, indicating wear rate became independent of the original MoS$_2$ inhomogeneity. Moreover,

the wear rates of the Cu–MoS$_2$ coating were as low as that of the pure Cu coating, yet contained a higher fluctuation, as evidenced by their higher standard deviation.

### 3.5 Raman Spectra on the Counterfaces and Wear Tracks

Figure 9a shows micrographs of the counterface mating with the Cu–MoS$_2$ coating after 100 cycles. Compacted wear debris adhered to the left and right edges of the contact, as expected in reciprocating sliding. Using Raman spectroscopy, the debris was identified as containing MoS$_2$; two characteristic peaks at around 400 cm^{-1} were detected, as seen in Fig. 9c. However, at the center of the contact, MoS$_2$ was not detected. MoS$_2$ is a very Raman active compound, where researchers commonly observe peaks even for very thin layers of a few nanometers [19]. Thus, while one can see flakes of debris attached to the counterfaces in Fig. 9a, b, no evidence was found for a significant presence of MoS$_2$ attached to the central contact of the counterface. At 1000 cycles, more wear debris maybe loose, collected mostly at the up and down edges of the contact (Fig. 9b). Raman analysis showed the presence of both MoS$_2$ and Cu$_2$O (Fig. 9d). The Cu$_2$O was identified by the peaks at low and high Raman shift range (below 300 and above 600 cm^{-1}) [20]. The compacted MoS$_2$-

Fig. 6 Top-down observation of the Cu wear track after the 100 cycle test. **a** overall morphology (*dashed lines* indicate wear track boundaries); **b** wear track topography; **c** spatial friction along the wear track at 100 cycles; **d** a closer view of the wear track. Refer to the scale bar in **a** for **a**, **b**, and **c**. SD indicates sliding direction
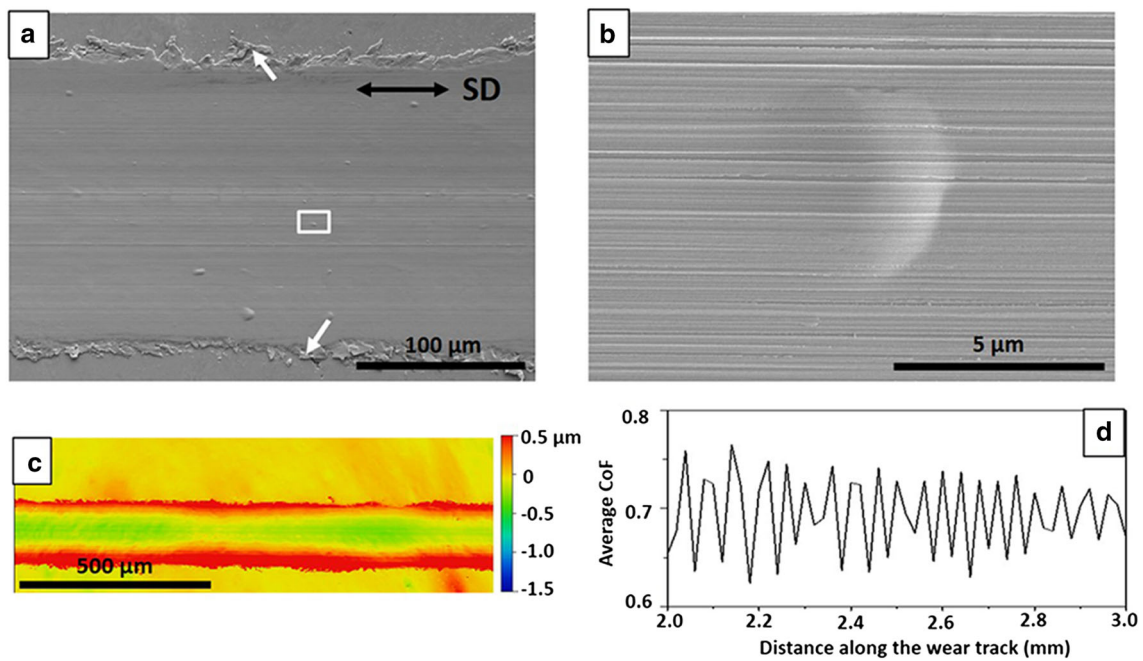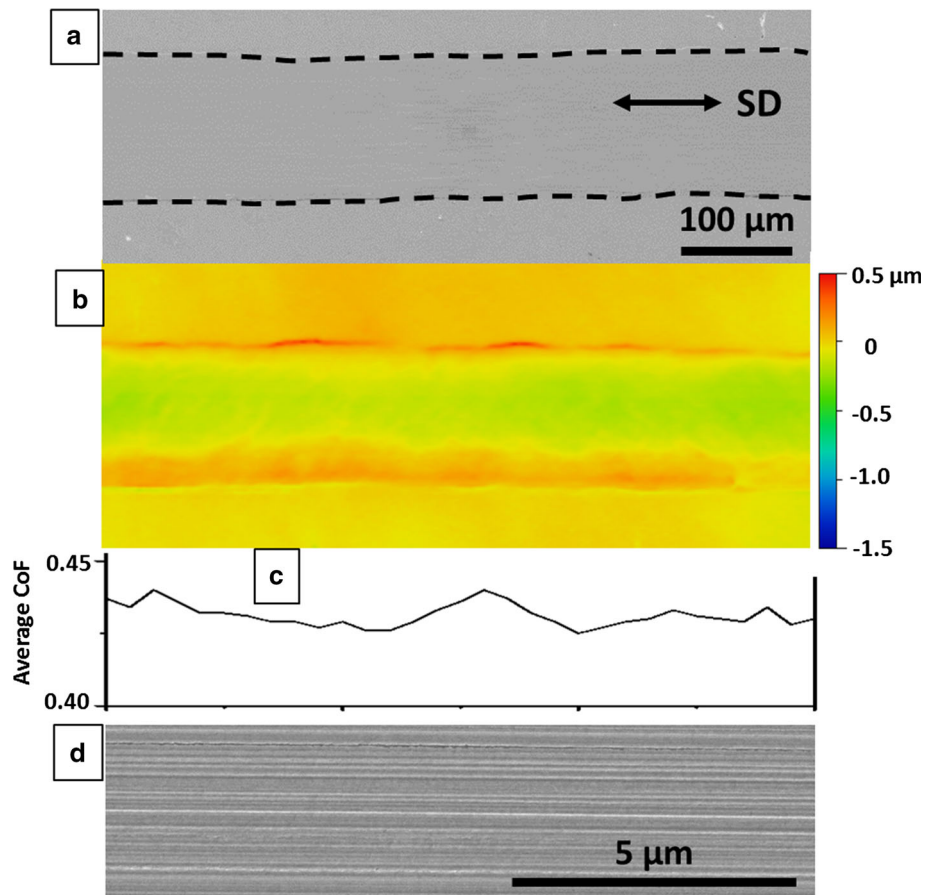
Fig. 7 Micrographs of top-down view of the Cu wear track after the 1000 cycle test. **a** Overall morphology, where the *white arrows* indicate extruded wear debris; **b** a closer view of the white rectangle in (**a**); **c** typical wear track topography; **d** spatial friction along the wear track at 1000 cycles. SD indicates sliding direction
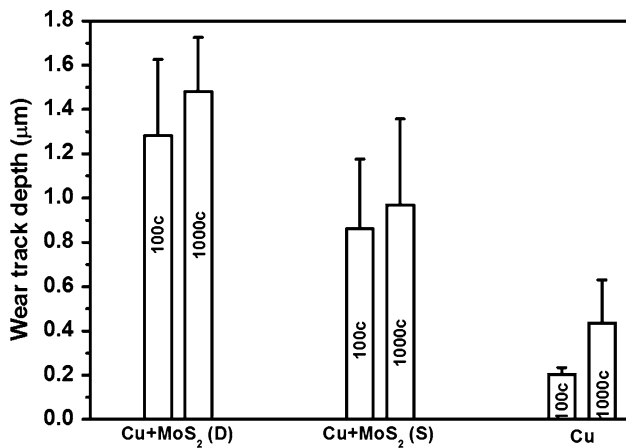
Fig. 8 Wear track depths of deep (*D*) and shallow (*S*) zones of Cu–MoS$_2$ and Cu coatings after the 100 and 1000 cycle tests. *Minus error bars are omitted for visual simplicity*

Table 1 Mean wear rates

Coatings	Wear rate (nm/cycle)	
	0–100 cycles	100–1000 cycles
Cu–MoS$_2$ (D)	12.8 ± 3.41	0.22 ± 0.47
Cu–MoS$_2$ (S)	8.61 ± 3.15	0.12 ± 0.55
Cu	2.04 ± 0.31	0.26 ± 0.22

containing wear debris found at 100 cycles was removed, and no MoS$_2$ was detected by Raman at the left and right edges of the contact. Figure 9e presents a Raman analysis on the corresponding wear tracks at 100 and 1000 cycles. MoS$_2$ was found in the patches mentioned previously in Fig. 5, which was consistent with the EDX map (Fig. 5d). Weak peaks corresponding to Cu$_2$O were also detected at such spots. At 1000 cycles, no MoS$_2$ but only Cu$_2$O peaks were obtained from the wear track.

For the Cu coating, Fig. 10 shows micrographs of the counterfaces and Raman analysis on both counterfaces and wear tracks. At 100 cycles, Cu color wear debris adhered at the contact (Fig. 10a), but no Raman active phases were detected (Fig. 10c). That indicates the transfer of Cu debris to the slider at the beginning of sliding. At 1000 cycles, a lot more wear debris was deposited at the periphery of the contact (Fig. 10b) and was identified as Cu$_2$O by Raman spectroscopy (Fig. 10d). It is worth noting that even though some of the wear debris looks like Cu, the surface might be oxidized as Cu$_2$O peaks were always detected. At the contact, however, most debris was still Cu (Fig. 10d). Raman analysis on the wear tracks, as shown in Fig. 10e, exhibited no Cu$_2$O formation at 100 cycles, yet oxidation took place over subsequent sliding as Cu$_2$O was detected at the 1000 cycle wear track.

3.6 Endurance of the First Steady-State Friction

In order to examine the endurance of the first steady-state of these two coatings, long tests of 3000 cycles were conducted. The average CoFs of Cu–MoS$_2$ and Cu coatings, plotted versus cycle number in Fig. 11, went beyond the steady-state and toward higher values of roughly 0.19 and 0.95, respectively. The rectangles in Fig. 11 show the endurance of the low friction, which was defined as the number of sliding cycles that the average CoF started climbing beyond the first steady-state values. The Cu–MoS$_2$ coating was able to endure up to around the 2250th cycle, whereas the Cu coating only stayed stable for approximately 1000 cycles. That indicated that the Cu–MoS$_2$ coating was able to withstand much more sliding cycles and thus achieve enhanced endurance of the first steady-state friction.

3.7 Sliding-Induced Microstructural Features

To study the role of MoS$_2$ on microstructural evolution over sliding, cross sections of the wear tracks were examined by the ECCI technique. Figure 12 shows the subsurface microstructure of Cu–MoS$_2$ coating after 3000 cycles. In the lower part of Fig. 12a, microstructure of original as-sprayed coatings was visible. It was highly deformed, as featured by deformation bands and tangled dislocations. Detailed microstructural features of as-sprayed coating were described elsewhere [21]. The initial cold spray particle boundaries were visible and shown as fine cracks within the matrix (Fig. 12a). The upper part of the micrograph showed near-surface microstructure that consists of a mechanically mixed layer (MML) and dynamic recrystallization layer (DRX). Interestingly, the MML appeared as islands, in which a mixture of ultrafine grains (UFG) and large grains (LG) were observed in a lamellar structure with fine cracks between the thin layers (Fig. 12b). The dark contrast in the UFG Cu was identified as rich in oxygen, indicating that oxidation occurred during sliding, which was consistent with the Raman spectroscopy observation. In the DRX layer, slightly relaxed microstructures were observed, as evidenced by an absence of deformation bands and tangled dislocations that showed in the as-sprayed microstructure. However, no significant grain growth was found. The depth of the sliding-induced microstructure varied in a range of 3–5 μm.

In contrast, a cross-sectional microstructure of Cu wear track after 3000 cycles shows dramatically different features (Fig. 13). The border of the sliding-induced microstructure was wavy and extended to a greater depth ranging from 10 to 30 μm. It also consists of the top layer of a MML, and a DRX layer underneath. In the MML, both UFG Cu and LG Cu were observed, as well as flakes of
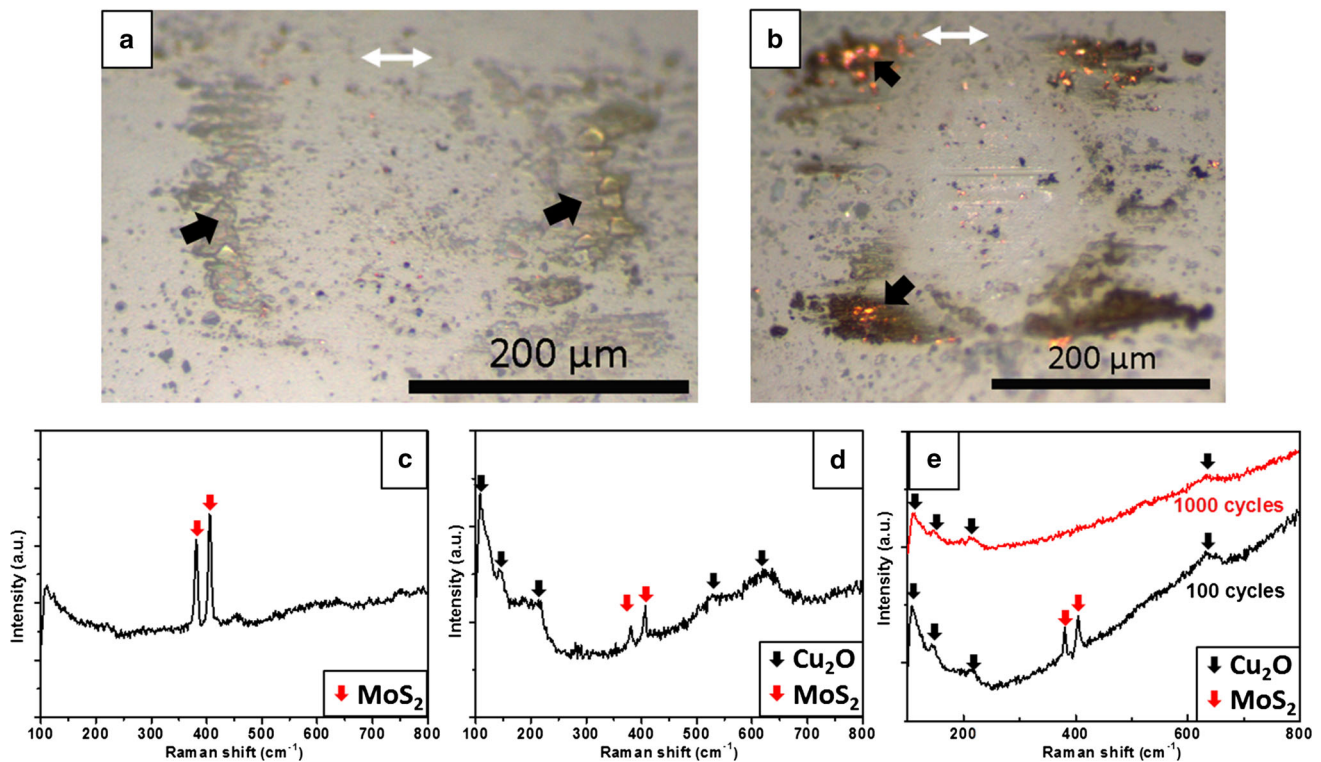
Fig. 9 Micrographs of the counterfaces mating with the Cu–MoS₂ coating after **a** 100 cycles and **b** 1000 cycles. Transferred patches and/or debris were found outside the contact, indicated as *black arrows*. Their Raman spectra were shown in (**c**) and (**d**), respectively. **e** Raman spectra taken from the wear track. *White arrows* indicate sliding direction

oxides (Fig. 13b). However, unlike the Cu–MoS₂ wear track, this MML did not show a fine lamellae configuration but a mixture of the above microstructures. Moreover, the MML was less coherent, as evidenced by a large amount of cracks (Fig. 13b). Some cracks were found to penetrate into the DRX layer (Fig. 13b). The DRX layer was more visible and exhibited relaxed and coarsened grains (Fig. 13a). Compared to the as-sprayed microstructure, dramatic grain growth was observed in the DRX layer and the grains seemed "clean" inside, indicative of an absence of defect contrast (Fig. 13b). This suggests low defect densities and thus well-developed recrystallized grains.

4 Discussion

In the present study, a cold-sprayed Cu–MoS₂ coating and Cu coating were subjected to dry sliding wear testing. The above results revealed that even though the MoS₂ concentration was only 1.8 ± 0.99 wt%, it was able to decrease the average friction coefficient significantly (from around 0.7 to 0.14–0.15). Furthermore, the local friction distribution combined with chemical analysis demonstrated that higher MoS₂ content zones generated lower local friction of 0.11–0.12 (Figs. 4a, c, 5a, c). In those zones,

MoS₂ was shown as fine debris and mixed with Cu and/or Cu₂O (Figs. 4e, 5e, 9e).

The mechanism for low friction in a metal–MoS₂ composite was expected to be slightly different from that found in blanket films of MoS₂ made by physical vapor deposition (PVD) or similar methods [1] [22–24]. The main feature of these latter coatings is to form transfer films on the counterbody, which leads to MoS₂ sliding versus MoS₂ and friction coefficients in the range of 0.02–0.06 in dry air at similar test conditions to those performed here [1]. Thus, while we found a significant friction reduction due to the presence of MoS₂, the mechanisms for this reduction were modified due to the presence of the Cu. The first noticeable difference was the lack of a transfer film observed at 100- and 1000-cycle tests (Fig. 9a, b). With only 1.8 wt% MoS₂ in the coating, any transfer films that did form were readily removed and redeposited onto the wear track. This was due to the interactions of MoS₂ with the wear track, which was primarily Cu—a very different contact condition compared to sliding on a PVD coating with a constant source of MoS₂. With the interactions of the metal, the transfer films were unstable and continuously removed, ultimately resulting in MoS₂ patches on the wear track that were expanded over sliding (Figs. 4d, 5d).
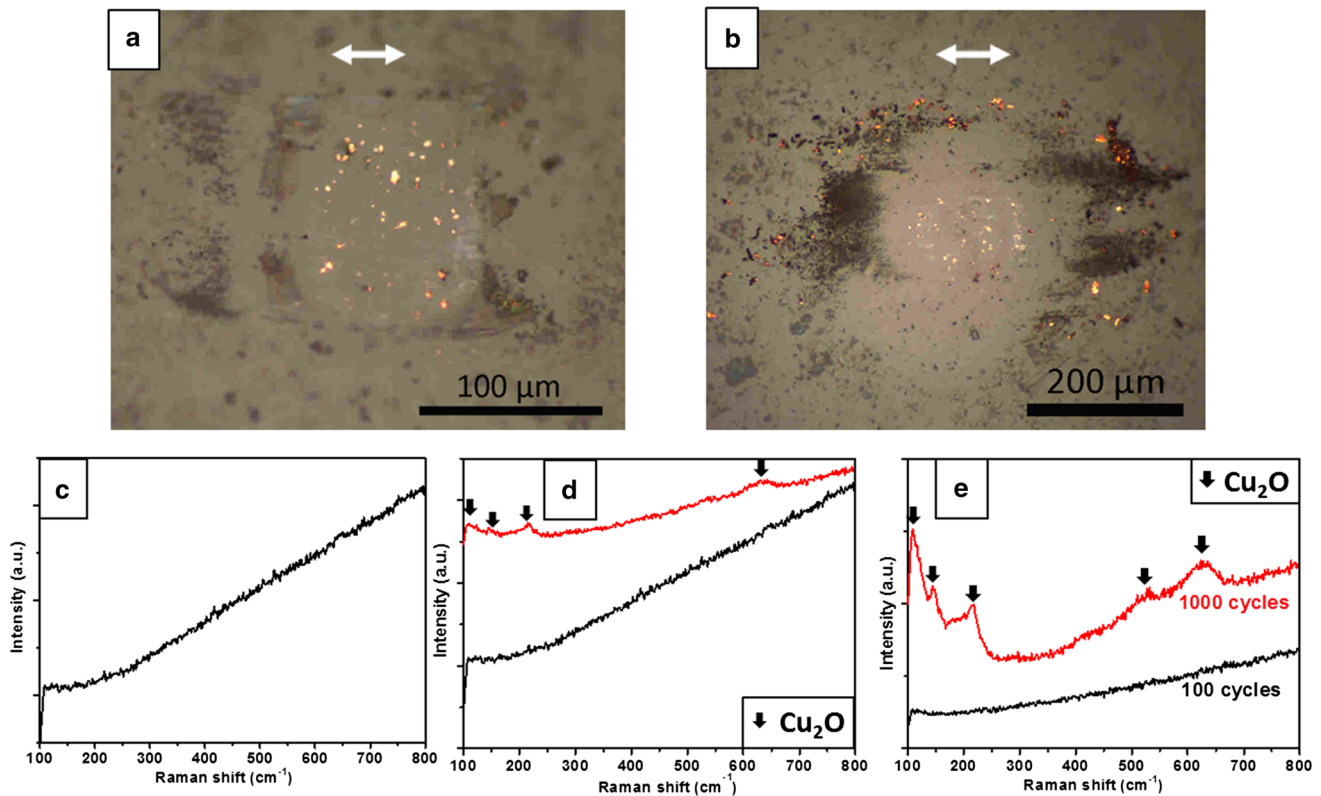
Fig. 10 Micrographs of the counterfaces mating with the Cu coating after **a** 100 cycles and **b** 1000 cycles. Transferred patches and/or debris were found on the counterfaces and their Raman spectra were shown in (**c**) and (**d**), respectively. The *black line* in (**d**) indicates Raman spectrum from the contact, while the *red one* the debris outside the contact. **e** Raman spectra taken from the wear track. *White arrows* indicate sliding direction (Color figure online)
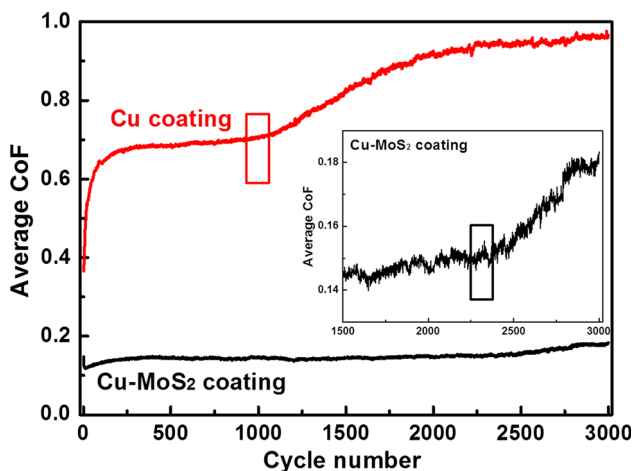

Fig. 11 Average coefficient of friction versus cycle number on cold-sprayed Cu–MoS$_2$ and Cu coatings. *Rectangles* indicate the cycle numbers where CoFs go beyond the first steady-state values

Using the two-term friction model that is commonly employed to combine two velocity accommodation mechanisms with an assumption that interaction between the friction mechanisms is negligible [25], the total friction can be written as:

$$\mu = \mu_{int} + \mu_{fracture} \tag{1}$$

where μ_{int} is friction from interfacial sliding and $\mu_{fracture}$ is the friction from fracture. Dvorak et al. [26] proposed a similar model for taking account of two friction mechanisms in MoS$_2$. In our study, the low MoS$_2$ content in the coating and the absence of a persistent MoS$_2$ transfer film on the counterface indicate that interfacial sliding between MoS$_2$ and MoS$_2$ did not occur to any great extent. The process by which the transfer films were removed and deposited back to the wear track as powdery MoS$_2$ was primarily related to the fracture of MoS$_2$. So the velocity difference was mostly accommodated by fracturing of MoS$_2$ third bodies. Therefore, $\mu_{int} \cong 0$, and $\mu \cong \mu_{fracture}$. Uemura et al. [27] demonstrated that fracture-dominated friction was 3–4 times higher than interfacial sliding (i.e., $\mu_{fracture} \cong 3.5 * \mu_{int}$). Also, Dvorak et al. [26] showed that the friction induced by interfacial sliding in dry air (i.e., $\mu \cong \mu_{int}$) under a wide range of contact pressure (0.41–1.39 GPa) was below 0.05. Thus, based on the results of Uemura and Dvorak, an estimate of fracture-induced friction indicated that it should be roughly 0.18 or below. This estimate was in a good agreement with the present study, where the friction of the high MoS$_2$ zones
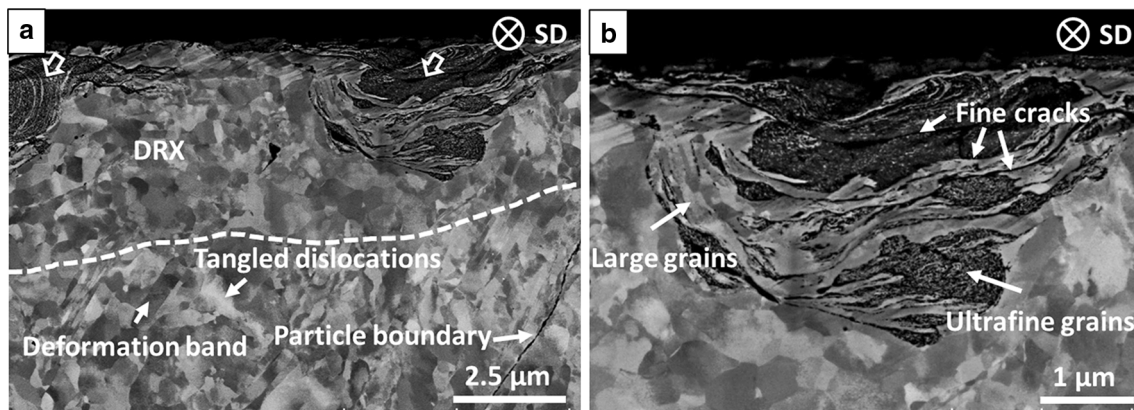
Fig. 12 a Micrograghs of cross section of the Cu–MoS$_2$ wear track after a 3000 cycle test. The *hollow arrows* denote MML, and the *dashed line* the border of the sliding-induced microstructure and as- sprayed microstructure. **b** A closer view of the sliding-induced microstructure. SD indicates sliding direction
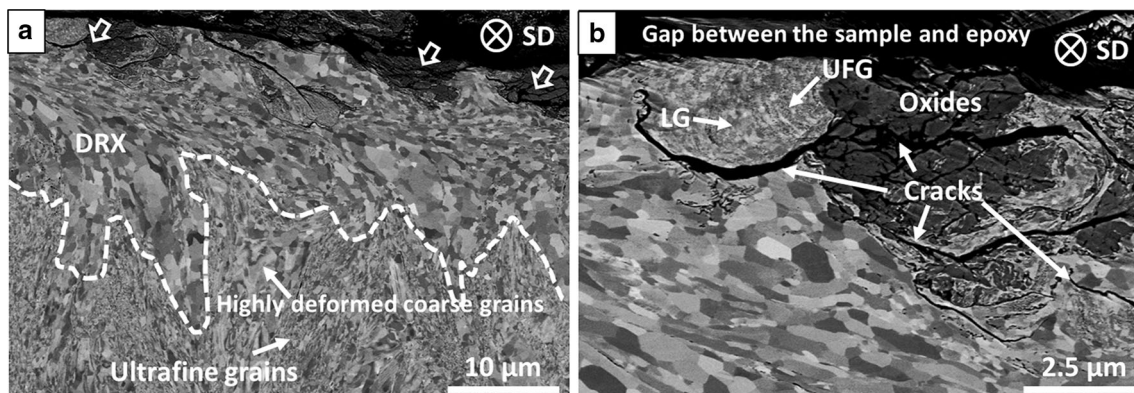
Fig. 13 a Micrograghs of cross section of the Cu wear track after a 3000 cycle test. The *hollow arrows* denote MML, the *dashed line* the border of the sliding-induced microstructure and the as-sprayed microstructure. **b** A closer view of the sliding-induced microstructure. SD indicates sliding direction

was 0.11–0.12. This analysis helped to understand how low friction can be observed with MoS$_2$ through a primarily fracture-based process instead of interfacial shearing. However, the elevated friction compared to an interfacial sliding mechanism must also partly be due to the occurrence of some metallic friction, evidenced by sliding grooves at the zones with little/no MoS$_2$ (Fig. 4e), and oxidation (Fig. 9e).

The pure Cu coating shows high friction throughout the wear tracks (Figs. 6c, 7c). Continuous sliding grooves parallel to the sliding direction were found in both 100 and 1000 cycle wear tracks (Figs. 6d, 7d). That could be due to abrasive wear induced by the Cu debris in the contact area of the counterfaces, as well as hard asperities of the counterfaces. Accompanied with oxidation, the velocity difference was accommodated by shearing within Cu and/ or Cu$_2$O, which introduced higher shear strength and thus higher friction. A similar material transfer process was observed previously in Cu bulk material in dry air [28].

Even though the presence of MoS$_2$ produced lower CoF zones, they, as well, introduced deeper wear tracks even after a short sliding period such as 100 cycles and therefore caused a higher wear. A MoS$_2$-induced mechanical property loss could be the main reason as it contributed to a poor ability to withstand high contact pressures and high wear. This has been observed elsewhere in self-lubricating composites. Dhanasekaran et al. [5] showed a 3 wt% addition of MoS$_2$ to Fe–C–Cu alloy achieved optimized friction and wear resistance, while 5 wt% MoS$_2$ caused high wear due to decreased strength. Kato et al. [6] found consistently decreased hardness and wear resistance with MoS$_2$ content higher than 10 vol% in copper–tin-based composites.

Lower wear was observed over subsequent sliding and became independent of initial MoS$_2$ inhomogeneity, which could be due to buildup and depletion of MoS$_2$ patches in the contact. In the early sliding, due to mechanical mixing and material transfer, MoS$_2$, originally accumulated along

particle boundaries, formed patches on the wear track locally (Fig. 4a). Some MoS_2 was transferred onto the counterface and collected at the left and right edges of the contact (Fig. 9a). As sliding proceeded and the contact area extended, the MoS_2 patches on the counterface were trapped back to the sliding contact and served as reservoirs to replenish MoS_2 loss. However, with oxidation and further mixing with Cu over sliding, the local MoS_2 concentration decreased gradually, as evidenced by the fact that it was too low to be detected by Raman (Fig. 9e) even though it was still visible by EDX technique (Fig. 5d). This also implies MoS_2 underneath the wear track might not be able to be brought up to the sliding contact, which could be due to the low concentration of MoS_2 but also due to the generally low wear rate of the coatings at the test conditions studied here. A similar process was found in previous studies on MoS_2 coatings. Wahl et al. [1] have shown how worn MoS_2 debris can be redistributed to the sliding contact as transfer film and/or tribofilm, as well as the important role of lubricant replenishment process on a final long period of low wear rate in a MoS_2 coating even though an initial rapid wear takes place.

The presence of MoS_2 helped to maintain the first steady-state friction for a longer period of time (Fig. 11) and to stabilize wear track morphology (Figs. 12, 13). Kovalchenko et al. [10] have demonstrated that endurance depends on solid lubricant content and the transition point delays with MoS_2 content. In the present study, cross-sectional microstructures of the wear tracks allow better understanding of the influence of MoS_2 on the improved endurance of the low friction. In both coatings, sliding led to changes in the microstructure and phase composition. For the Cu–MoS_2 wear track, sliding induced a cohesive lamellae MML with fine cracks and a shallow DRX layer 3–5 µm deep, where a decrease in defect density was observed but no significant grain growth. However, for the Cu wear track, sliding introduced large cracks within the MML. The DRX layer penetrated into the coating as deep as 10–30 µm, and substantial grain growth was found in the DRX layer. There were several possible reasons for those significant differences. First, it could be primarily related to the stress field induced by shearing. Rupert et al. [29] demonstrated in a nanocrystalline Ni–W alloy that subsurface microstructural evolution such as grain growth and grain boundary relaxation is mainly produced by local shear stress. In the present study, for the Cu–MoS_2 coating, generation of MoS_2-containing debris on the wear track separated the initial contact, and friction force was subsequently carried by the debris. Therefore, stress imposed onto the underlying material could be very low. In contrast, when rubbing against the pure Cu coating, as discussed previously, shearing occurred mostly within the subsurface of the wear track by plastic deformation, which could cause

a strong stress field comparing to the lubricated case. The stress field calculated by numerical approach also demonstrated that the von Mises stress beneath the contact, which plays an important role in deformation-induced microstructural change [30], and increases with friction [31]. This could interpret the difference in subsurface microstructures of those two coatings. Moreover, frictional heating might play a role as well. Yao et al. [28] have demonstrated that sliding tests performed within liquid nitrogen do not induce grain growth within the DRX layer compared to that under room temperature. When rubbing against the Cu–MoS_2 coating, less heat was generated at the contact due to its low friction, and it was not surprising that no significant microstructural change in the subsurface occurred. In addition, mild oxidation occurred in the Cu–MoS_2 wear tracks even after a long term sliding of 3000 cycles, while much heavier oxidation in the pure Cu wear tracks (Figs. 12, 13). This seems also due to the influence of MoS_2, which is found to be able to shield the underneath material from interaction with environment [32]. In general, due to the presence of MoS_2, minor changes in subsurface microstructure and phase transformation were found in the Cu–MoS_2 wear track compared to Cu wear track.

5 Conclusions

A Cu–MoS_2 composite coating was fabricated by cold spray, and its dry sliding wear performance was studied and compared to a Cu coating. The Cu–MoS_2 coating exhibited much lower overall friction coefficient, with local friction controlled by local MoS_2 concentration. The velocity difference was primarily accommodated by fracturing of MoS_2 third bodies.

The MoS_2-rich zones caused high wear at the beginning, which could be due to its decreased hardness. However, low wear rates (0.12 and 0.22 nm/c in average) were found throughout the whole wear track over the subsequent sliding, independent of local MoS_2 content, that could be due to a MoS_2 replenishment and depletion process during sliding.

The presence of MoS_2 also contributed to the enhanced endurance of the first steady-state friction in the Cu–MoS_2 coating. The friction started climbing at around 2250 cycles, while the Cu coating stayed stable only up to roughly 1000 cycles.

Cross-sectional micrographs of the wear tracks revealed that minor modifications in terms of subsurface microstructure and phase transformation occurred in the Cu–MoS_2 coating compared to the Cu coating after 3000 cycles. It was found in the Cu–MoS_2 wear track, there was a cohesive lamellae MML with fine cracks and a shallow

DRX layer 3–5 μm deep. Even though a decrease in dislocation density was observed in the DRX layer, no significant grain growth took place. However, sliding produced a wavy and deep MML and DRX layer in the Cu coating. A large amount of cracks and oxides were found in the MML and significant grain growth in the DRX layer. Those differences could be related to a sliding-induced stress field and frictional heating.

References

1. Wahl, K.J., Singer, I.L.: Quantification of a lubricant transfer process that enhances the sliding life of a MoS$_2$ coating. Tribol. Lett. **1**, 59–66 (1995)
2. Martin, J.M., Donnet, C., Le Mogne, T., Epicier, T.: Superlubricity of molybdenum disulphide. Phys. Rev. B **48**(14), 10583–10586 (1993)
3. Dudder, G.J., Zhao, X., Krick, B., Sawyer, W.G., Perry, S.S.: Environmental effects on the tribology and microstructure of MoS$_2$–Sb$_2$O$_3$–C films. Tribol. Lett. **42**, 203–213 (2011)
4. Lansdown, A.R.: Tribology Series. Elsevier, Amsterdam (1999)
5. Dhanasekaran, S., Gnanamoorthy, R.: Dry sliding friction and wear characteristics of Fe–C–Cu alloy containing molybdenum disulphide. Mater. Des. **28**, 1135–1141 (2007)
6. Kato, H., Takama, M., Iwai, Y., Washida, K., Sasaki, Y.: Wear and mechanical properties of sintered copper–tin composites containing graphite or molybdenum disulfide. Wear **255**, 573–578 (2003)
7. Du, H., Sun, C., Hua, W., Wang, T., Gong, J., Jiang, X., Lee, S.W.: Structure, mechanical and sliding wear properties of WC–Co/MoS$_2$–Ni coatings by detonation gun spray. Mater. Sci. Eng. A **445–446**, 122–134 (2007)
8. Du, H., Sun, C., Hua, W.G., Zhang, Y.S., Han, Z., Wang, T.G., Gong, J., Lee, S.W.: Fabrication and evaluation of D-gun sprayed WC–Co coating with self-lubricating property. Tribol. Lett. **23**, 261–266 (2006)
9. Yuan, J., Zhu, Y., Zheng, X., Ji, H., Yang, T.: Fabrication and evaluation of atmospheric plasma spraying WC–Co–Cu–MoS$_2$ composite coatings. J. Alloys Compd. **509**, 2576–2581 (2011)
10. Kovalchenko, A.M., Fushchich, O.I., Danyluk, S.: The tribological properties and mechanism of wear of Cu-based sintered powder materials containing molybdenum disulfide and molybdenum diselenite under unlubricated sliding against copper. Wear **290–291**, 106–123 (2012)
11. Champagne, V.K.: The Cold Spray Materials Deposition Process: Fundamentals and Applications. Woodhead, Cambridge (2007)
12. Irissou, E., Jean-Gabriel, L., Anatoly, R., Bertrand, J., Christian, M.: Review on cold spray process and technology: part I-intellectual property. J. Therm. Spray Technol. **17**, 495–516 (2008)
13. Assadi, H., Gartner, F., Stoltenhoff, T., Kreye, H.: Bonding mechanism in cold gas spraying. Acta Mater. **51**, 4379–4394 (2003)
14. Bae, G., Kumar, S., Yoon, S., Kang, K., Na, H., Kim, H., Lee, C.: Bonding features and associated mechanisms in kinetic sprayed titanium coatings. Acta Mater. **57**, 5654–5666 (2009)
15. Grujicic, M., Pandurangan, B., Bell, W.C., Daqaq, M., Ma, L., Seyr, N., Erdmann, M., Holzleitner, J.: A computational analysis and suitability assessment of cold-gas dynamic spraying of glass-fiber-reinforced poly-amide 6 for use in direct-adhesion polymer metal hybrid components. Appl. Surf. Sci. **254**(7), 2136–2145 (2008)
16. Smid, I., Segall, A.E., Walia, P., Aggarwal, G., Eden, T.J., Potter, J.K.: Cold-sprayed Ni-hBN self-lubricating coatings. Tribol. Trans. **55**, 599–605 (2012)
17. Yamada, M., Wakabayashi, J., Fukumoto, M., Kitamura, J.: Fabrication of Cu–MoS$_2$ composite coating by cold spraying and evaluation of its property. In: Marple, B.R., Hyland, M.M., Lau, Y.-C., Li, C.-J., Lima, R.S., Montavon, G. (eds.) Proceedings of the International Thermal Spray Conference 2009, pp. 326–330 (2009)
18. Strauss, H.W., Chromik, R.R., Hassani, S., Klemberg-Sapieha, J.E.: In situ tribology of nanocomposite Ti–Si–C–H coatings prepared by PE-CVD. Wear **272**, 133–148 (2011)
19. Liu, K.-K., Zhang, W., Lee, Y.-H., Lin, Y.-C., Chang, M.-T., Su, C.-Y., Chang, C.-S., Li, H., Shi, Y., Zhang, H., Lai, C.-S., Li, L.-J.: Growth of large-area and highly crystalline MoS$_2$ thin layers on insulating substrates. Nano Lett. **12**(3), 1538–1544 (2012)
20. Hessea, J.F., Compaan, A.: Resonance Raman studies of annealing in He-, Na-, Cd-implanted cuprous oxide. J. Appl. Phys. **50**, 206–213 (1979)
21. Zhang, Y., Brodusch, N., Descartes, S., Chromik, R.R., Gauvin, R.: Microstructure refinement of cold-sprayed copper investigated by electron channeling contrast imaging. Microsc. Microanal. **20**, 1499–1506 (2014)
22. Lince, J.R.: Tribology of co-sputtered nanocomposite Au/MoS$_2$ solid lubricant films over a wide contact stress range. Tribol. Lett. **17**(3), 419–428 (2007)
23. Stoyanov, P., Strauss, H.W., Chromik, R.R.: Scaling effects between micro- and macro-tribology for a Ti–MoS$_2$ coating. Wear **274–275**, 149–161 (2012)
24. Wahl, K.J., Chromik, R.R., Lee, G.Y.: Quantitative in situ measurement of transfer film thickness by a Newton's rings method. Wear **264**, 731–736 (2008)
25. Bowden, F.P., Tabor, D.: The Friction and Lubrication of Solids. Clarendon, Oxford (1986)
26. Dvorak, S.D., Wahl, K.J., Singer, I.L.: In Situ analysis of third body contributions to sliding friction of a Pb–Mo–S Coating in dry and humid air. Tribol. Lett. **28**, 263–274 (2007)
27. Uemura, M., Okada, K., Mogami, A., Okitsu, A.: Effect of friction mechanisms on friction coefficient of MoS$_2$ in an ultrahigh-vacuum. Lubric. Eng. **43**, 937–942 (1987)
28. Yao, B., Han, Z., Lu, K.: Dry sliding tribological properties and subsurface structure of nanostructured copper at liquid nitrogen temperature. Wear **301**, 608–614 (2013)
29. Rupert, T.J., Schuh, C.A.: Sliding wear of nanocrystalline Ni–W: structural evolution and the apparent breakdown of Archard scaling. Acta Mater. **58**, 4137–4148 (2010)
30. Rupert, T.J., Gianola, D.S., Gan, Y., Hemker, K.J.: Experimental observations of stress-driven grain boundary migration. Science **326**, 1686–1690 (2009)
31. Hamilton, G.M.: Explicit equations for the stresses beneath a sliding spherical contact. Proc. Inst. Mech. Eng. C **197**, 53–59 (1983)
32. Rigney, D.A.: Comments on the sliding wear of metals. Tribol. Int. **30**, 361–367 (1997)